Development 137, 1263-1273 (2010) doi:10.1242/dev.045625

Cell migration that orients the dorsoventral axis is coordinated with anteroposterior patterning mediated by Hedgehog signaling in the early spider embryo

Yasuko Akiyama-Oda* and Hiroki Oda*

SUMMARY

The early embryo of the spider *Achaearanea tepidariorum* is emerging as a model for the simultaneous study of cell migration and pattern formation. A cell cluster internalized at the center of the radially symmetric germ disc expresses the evolutionarily conserved dorsal signal Decapentaplegic. This cell cluster migrates away from the germ disc center along the basal side of the epithelium to the germ disc rim. This cell migration is thought to be the symmetry-breaking event that establishes the orientation of the dorsoventral axis. In this study, knockdown of a *patched* homolog, *At-ptc*, that encodes a putative negative regulator of Hedgehog (Hh) signaling, prevented initiation of the symmetry-breaking cell migration. Knockdown of a *smoothened* homolog, *At-smo*, showed that Hh signaling inactivation also arrested the cells at the germ disc center, whereas moderate inactivation resulted in sporadic failure of cell migration termination at the germ disc rim. *hh* transcript expression patterns indicated that the rim and outside of the germ disc were the source of the Hh ligand. Analyses of patterning events suggested that in the germ disc, short-range Hh signal promotes anterior specification and long-range Hh signal represses caudal specification. Moreover, negative regulation of Hh signaling by *At-ptc* appears to be required for progressive derepression of caudal specification from the germ disc center. Cell migration defects caused by *At-ptc* and *At-smo* knockdown correlated with patterning defects in the germ disc epithelium. We propose that the cell migration crucial for dorsoventral axis orientation in *Achaearanea* is coordinated with anteroposterior patterning mediated by Hh signaling.

KEY WORDS: Axis formation, Cell migration, Patched, Hedgehog, Smoothened, Dpp, RNAi, *Achaearanea tepidariorum*, Spider

INTRODUCTION

The migration of a signaling source is a common strategy for directing the activation or inhibition of a signaling pathway in the appropriate regions during animal development. Such migration must be regulated in concert with ongoing pattern formation to achieve the correct cell-cell interactions (Solnica-Krezel, 2005; Tam et al., 2006). Although the molecular machinery and guiding factors underlying cell migration have been studied using in vitro culture systems and in vivo model systems (Cram et al., 2006; Simpson et al., 2008; Wang et al., 2006), there are few systems that allow simultaneous study of cell migration and pattern formation.

The migration of cells serving as the signaling source is crucial for formation of the embryonic axis in some model organisms. During egg cylinder development in mouse, the distal visceral endoderm cells, which express antagonists of Nodal and Wnt (Kimura-Yoshida et al., 2005; Yamamoto et al., 2004), migrate towards the future anterior side (Beddington and Robertson, 1999). This cell migration is one of the earliest steps in axis formation in mouse, and the importance of the signaling molecules has been established genetically. However, accessibility to the migration and patterning events in mouse egg cylinders is limited.

Early spider embryos, like the mouse embryo, exhibit the migration of a cellular source that secretes signaling molecules. In the house spider *Achaearanea tepidariorum*, which is emerging as a model organism (Oda and Akiyama-Oda, 2008), a cluster of endoderm cells, termed the cumulus mesenchymal (CM) cells, is internalized from the blastopore and migrates on the basal surface of the static germ disc epithelium (see Fig. 1A) (Akiyama-Oda and Oda, 2003). The migratory CM cells and the associated surface epithelial cells can be easily observed as a distinct white spot that is conventionally called the cumulus. The CM cells express a homolog of *decapentaplegic*, *At-dpp*, that encodes the evolutionarily conserved dorsal signal (Akiyama-Oda and Oda, 2003). During migration, the Dpp signal from the CM cells affects the surface epithelium: in these cells, the transcription factor Mothers against dpp (Mad) is phosphorylated and translocated to the nucleus (Fig. 1B).

During spider development, the formation and migration of the CM cells is preceded by the formation of a single embryonic axis termed the embryonic-abembryonic (Em-Ab) axis (Fig. 1A). Centrifugal migration of the CM cells from the Em polar region is the first morphological sign of dorsoventral (D-V) axis formation. No molecular asymmetries that indicate the direction of CM cell migration have yet been identified. As the CM cells arrive at a site on the germ disc rim, the surrounding epithelial cells begin to differentiate into extraembryonic tissue, signifying the dorsal side of the developing embryo. The extraembryonic tissue rapidly expands as the germ disc transforms into a germ band in which the anteroposterior (A-P) and D-V axes become evident. The anterior and caudal regions of the forming germ band appear to be related to the peripheral and central regions, respectively, of the germ disc. Our previous study using parental RNA interference (RNAi) showed that the Dpp signal is essential for extraembryonic tissue formation and D-V axis polarization, although the CM cell migration itself might not require this signal (Akiyama-Oda and Oda, 2006). Because of the easily visible cell migration and its functional importance in axis

JT Biohistory Research Hall, 1-1 Murasaki-cho, Takatsuki, Osaka 569-1125, Japan.

*Authors for correspondence (yasuko@brh.co.jp; hoda@brh.co.jp)

Accepted 3 February 2010

formation, as well as the availability of parental RNAi, the early spider embryo offers an invaluable opportunity to study cell migration and pattern formation simultaneously.

In this study, we conducted a pilot screen for genes involved in CM cell migration in the *Achaearanea* embryo. We found that components of the Hedgehog (Hh) signaling pathway are required for CM cell migration, germ disc patterning and axis formation. Based on these results, we propose a model in which CM cell migration is coordinated with pattern formation mediated by Hh signaling.

MATERIALS AND METHODS

Spiders

Laboratory stocks of the house spider *Achaearanea tepidariorum* were maintained at 25°C. Every mated female was evaluated by monitoring the development of embryos in the first egg sac; only those that produced healthy eggs were used in experiments. Developmental stages were described previously (Akiyama-Oda and Oda, 2003; Yamazaki et al., 2005). Malformed embryos following RNAi treatment were staged based on the time past stage 4. In the experiments in which early embryos were used, the development of sibling embryos derived from the same egg sacs was checked later to confirm that consistent results were observed.

cDNAs

For information about the cDNAs used in this study, see Table S1 in the supplementary material. cDNA fragments of *At-ptc*, *At-smo*, *At-labial* (*At-lab*) and *At-gataC* were originally isolated by PCR using degenerate primers (see Table S2 in the supplementary material). Longer cDNA clones were then isolated by 5′ and 3′ RACE using a SMART RACE cDNA Amplification Kit (Clontech, Mountain View, CA, USA). Primers used for RACE are shown in Table S2 in the supplementary material. Phylogenetic trees were constructed for Ptc and Smo by the neighbor-joining method (Saitou and Nei, 1987) using PHYLIP 4.0 (see Fig. S1 in the supplementary material). The nucleotide sequences reported here are available in the DDBJ/EMBL/GenBank databases under the accession numbers AB433900-AB433908 and AB524079.

Parental RNAi

The 709 bp (nt 1-709) and 720 bp (nt 706-1425) regions of *At-ptc* cDNA, the 1020 bp (nt 1-1020) and 924 bp (nt 1017-1940) regions of *At-hh* cDNA, the 633 bp (nt 1543-2175) and 823 bp (nt 2176-2998) regions of *At-smo* cDNA and the entire coding region of *green fluorescent protein* (*gfp*) cDNA (Quantum) were used to synthesize *At-ptc1*, *At-ptc2*, *At-hh1*, *At-hh2*, *At-smo1*, *At-smo2* and *gfp* double-stranded (ds) RNAs, respectively. *gfp* dsRNA was used as the control. *At-Delta*^{HH} dsRNA was prepared as described previously (Oda et al., 2007). dsRNAs were synthesized as described (Akiyama-Oda and Oda, 2006) and were used at 1.5-2.0 μg/μl for injection. Females were given four injections of dsRNA solution (1-2 μl each) at 2- to 3-day intervals, except for five females: one for *At-smo1* and two for *At-smo2* were each given three injections; one for *At-smo1* and one for *At-Delta*^{HH} were given six and five injections, respectively. For simultaneous RNAi against two genes (double RNAi), females were given a total of eight injections (one dsRNA solution after the other) at 2- to 3-day intervals.

Reverse-transcription (RT) PCR

Each pool of mRNA was prepared from 30-60 embryos using the QuickPrep Micro mRNA Purification Kit (GE Healthcare, UK). Synthesis of first-strand cDNA was performed using random primers and SuperScript III reverse transcriptase (Invitrogen, Carlsbad, CA, USA), followed by PCR using ExTaq polymerase (Takara, Shiga, Japan). The PCR conditions were as follows: 95°C for 30 seconds; 25 or 30 cycles of 95°C for 5 seconds and 60°C for 20 seconds. Controls lacking reverse transcriptase in the cDNA synthesis reaction failed to produce specific products in all cases. Real-time PCR and quantification were performed using SYBR Premix ExTaq with a Thermal Cycler Dice Real-Time System TP800 (Takara). The PCR cycles were as above, followed by a dissociation cycle: 95°C for 15 seconds, 60°C for 30 seconds and 95°C for 15 seconds. The dissociation curves were examined to confirm the presence of the single expected product and the absence of non-specific products or primer dimers. The relative quantities were calculated by the crossing-point standard curve method. All real-time reactions were repeated several times. The nucleotide sequences (5′ to 3′) of the primer pairs were as follows: *At-ptc*, GCAGTAACTAC-CAGAGTTACAGC and CTTCTGGATGAGGAACTATCACG; *At-hh*, TGGTGTAGTAGCTTCCTGCTACG and TGTACCTGAGGATGTG-CATAGTC; *At-smo*, GATCATCTTGTGTGCCTTGC and TGATACAT-GTGGGCATTTGG; *At-ef1α*, CTGTACCAGGAGACAATG and ATC-TGACCAGGATGGTTC; *At-dpp*, CCGCATGAGAATTATGGACTGC and CGACTTGATTCCACCTATGAGG; *At-α-catenin*, ATGCAGCTC-GTATATTGG and CACCCTCTTGTAGAGCAA.

Embryo staining

Single and dual-color whole-mount in situ hybridization (WISH) and staining with antibody against phosphorylated Mad (pMad) (Persson et al., 1998) were performed as described previously (Akiyama-Oda and Oda, 2003). To detect FITC probes in dual-color WISH, alkaline phosphatase (AP)-conjugated rabbit anti-FITC (DAKO, 1:200 dilution) or sheep anti-fluorescein-AP (Roche, 1:1000) antibody was used. Most samples were counterstained with DAPI. Alexa Fluor 488 phalloidin (Molecular Probes, Eugene, OR, USA) was used for F-actin staining.

Time-lapse recording of live embryos

Preparation of embryos was as described previously (Oda et al., 2007). Images were acquired every 10 minutes using a stereomicroscope (SZX12, Olympus, Tokyo, Japan) equipped with a color CCD camera (C7780-10, Hamamatsu Photonics, Shizuoka, Japan) controlled by AquaCosmos software (Hamamatsu Photonics). Images were processed using ImageJ 1.42q, MetaMorph 6.1 and Adobe Photoshop CS2 software.

RESULTS

CM cell migration is concurrent with germ disc patterning

The CM cell cluster starts to migrate from the center of the germ disc at early stage 5 (Fig. 1A). Prior to the start of migration, scattered *At-Delta* expression appears around the germ disc center; this *At-Delta* expression is involved in caudal specification (Oda et al., 2007). We examined the relationship between the position of the CM cells and the pattern of *At-Delta* expression by dual-color WISH. A *singed*-related gene, 022_P10, was used as a marker of CM cells. As the *At-Delta* expression domain expanded symmetrically from the germ disc center, the CM cells shifted to an asymmetric position (Fig. 1C). In the majority of mid-stage 5 embryos, the migrating CM cells were positioned close to the border of the *At-Delta* expression domain. It appeared that CM cell migration was accompanied by dynamic expansion of gene expression starting from the germ disc center. However, the expansion of the *At-Delta* expression domain stopped at approximately half of the radius of the germ disc, whereas the CM cells continued to migrate until they reached the germ disc rim at late stage 5.

Injection of dsRNA targeting *At-ptc* results in a defective cumulus shift

To search for genes required for CM cell migration, we performed a pilot gene-knockdown screen. dsRNAs were prepared from more than 30 genes, most of which were originally isolated as homologs of *Drosophila* and/or vertebrate patterning genes (see Table S3 in the supplementary material). Each dsRNA was injected into adult females, and the live embryos they produced were observed under a stereomicroscope. In this initial screen, we identified only one candidate gene, *At-ptc*, a homolog of the *Drosophila* segment polarity gene *patched* (*ptc*). Injection of dsRNA targeting *At-ptc* (*At-ptc1* dsRNA) resulted in embryos in which the cumulus shift was prevented or largely delayed (Fig. 1D, Fig. 2D; see Movie 1 in the supplementary material). The penetrance of this phenotype was high (see Fig. S2 in the supplementary material). Until early stage 5, these

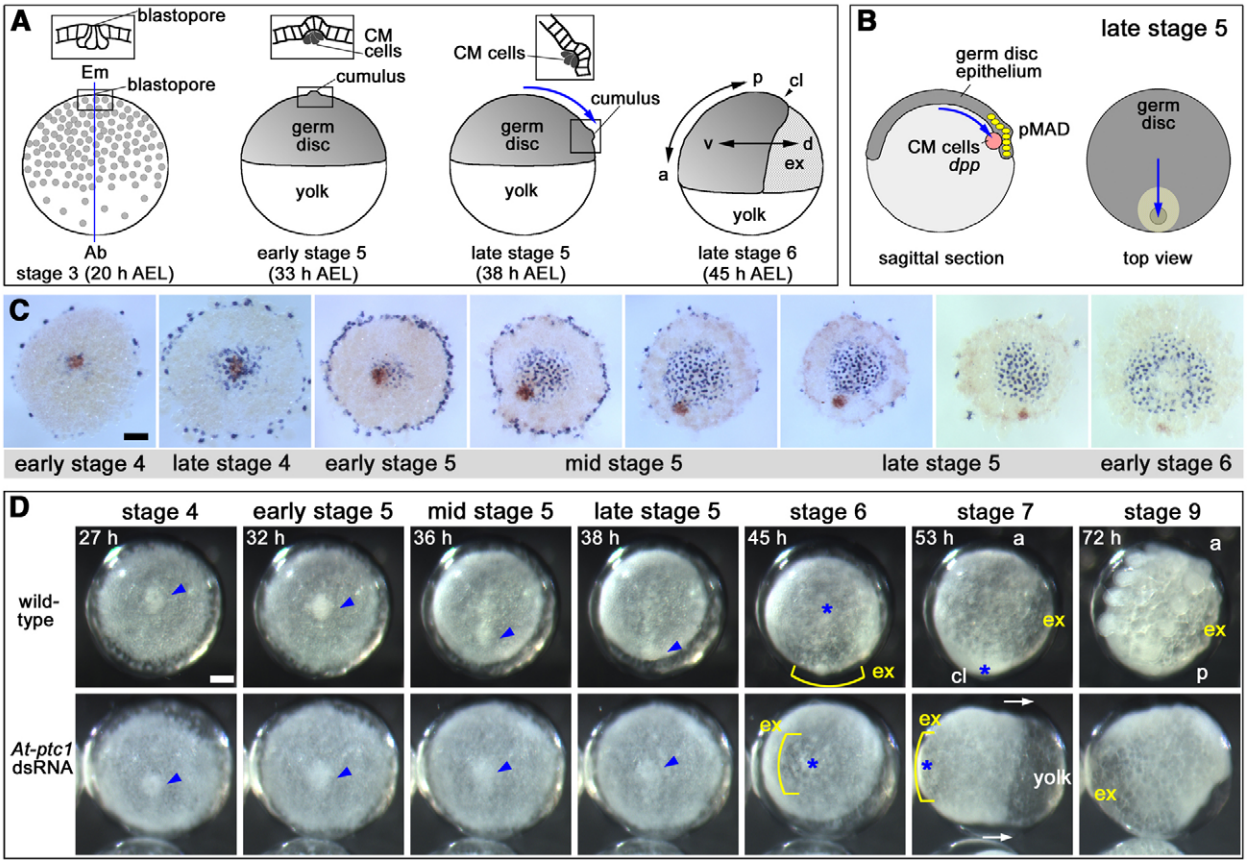

Fig. 1. The formation and migration of CM cells during early *Achaearanea* embryogenesis and cumulus-shift defects caused by *At-ptc1* dsRNA injection. (**A**) Schematic illustrations showing lateral views of *Achaearanea* embryos at the indicated stages. The boxed areas are magnified in the insets to show the internalization of endoderm cells from the blastopore (stage 3) and the location of clustered CM cells (early and late stage 5). The curved blue arrow indicates the direction of the cumulus shift. (**B**) Illustrations of a late stage 5 embryo. The CM cell cluster is shown in orange and pMad-positive nuclei are in yellow. Blue arrows indicate the migration of the CM cells. (**C**) Top views of flat-mounted germ discs double stained for *At-Delta* transcripts (purple) and the CM cell marker 022_P10 (red) at successive stages. (**D**) Time-lapse observation of wild-type and *At-ptc1* dsRNA-treated embryos. The embryo in the bottom row is the same as that in the upper right of the field in Fig. 2D. The approximate time (h, hours) after egg laying (AEL) is indicated. Arrowheads indicate the blastopore (stage 4) and cumulus (early, mid- and late stage 5). Both embryos rotated during stages 6 and 7; the asterisks mark identical points in sequential panels. White arrows indicate the directional movement of the embryonic cells in the *At-ptc1* dsRNA-treated embryo (stage 7). Em, embryonic pole; Ab, abembryonic pole; a, anterior; p, posterior; d, dorsal; v, ventral; ex, extraembryonic tissue; cl, caudal lobe. Scale bars: 100 μm.

embryos were morphologically indistinguishable from wild-type embryos. The prevention of cumulus shift was accompanied by the ectopic formation of extraembryonic tissue around the germ disc center. In extreme cases, the extraembryonic tissue spread over the Em hemisphere, with all embryonic cells shifted to the Ab side, resulting in a pear-shaped form.

To examine RNAi specificity, we prepared another dsRNA (*At-ptc2* dsRNA) from a different region of the *At-ptc* cDNA (see Fig. S2A in the supplementary material). Injection of *At-ptc2* dsRNA, but not control *gfp* dsRNA, yielded the same phenotype as *At-ptc1* dsRNA (see Fig. S2B in the supplementary material). Moreover, real-time PCR revealed specific reduction of the *At-ptc* transcript level, and WISH revealed reduced signals for the cytoplasmic pool of *At-ptc* transcripts (see Fig. S2C,D in the supplementary material). These results led us to conclude that specific suppression of *At-ptc* function resulted in prevention of the cumulus shift. Hereafter, embryos derived from females injected with *At-ptc* or *gfp* dsRNA are referred to as *At-ptc* or *gfp* RNAi embryos, respectively. Because the same results were obtained with *At-ptc1* and *At-ptc2* dsRNAs, only results obtained with *At-ptc1* are shown.

Knockdown of *At-hh* and *At-smo* also affects the cumulus shift

ptc encodes a membrane receptor for the secreted Hh signal (Fuse et al., 1999; Ingham et al., 1991; Marigo et al., 1996; Stone et al., 1996), and Ptc is thought to be a negative regulator of Hh signaling (Ingham et al., 1991; Taipale et al., 2002). In the absence of ligand, Ptc represses the activity of another membrane receptor, Smo (Alcedo et al., 1996; van den Heuvel and Ingham, 1996). When bound by Hh, Ptc no longer inhibits Smo, allowing Smo to transduce the Hh signal intracellularly (Hooper and Scott, 2005; Ingham and McMahon, 2001; Lum and Beachy, 2004). The removal of Ptc also leads to Smo activation even in the absence of Hh (Hooper and Scott, 2005).

To investigate the potential contribution of other components of the Hh signaling pathway to CM cell migration, we performed parental RNAi against the *Achaearanea* homologs of *hh* and *smo*. Two different dsRNAs were prepared for each gene (*At-hh1*, *At-hh2*, *At-smo1* and *At-smo2*; see Fig. S3 in the supplementary material). Injection of these four dsRNAs resulted in embryos that had similar phenotypes. This indicated that the phenotypes were specific effects of *At-hh* and *At-smo* knockdown and also implied that *At-hh* and *At-*

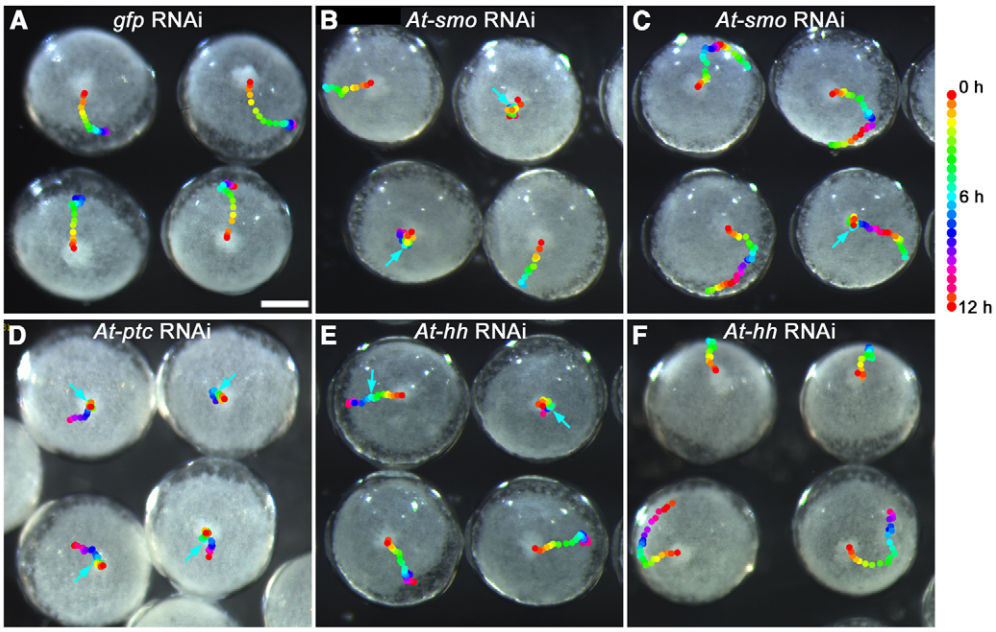

Fig. 2. Cumulus-shift defects in *At-smo*, *At-ptc* and *At-hh* RNAi embryos. (**A-F**) Cumulus movement from early stage 5 (~32 hours AEL) to stage 6 in *gfp* (A), *At-smo* (B,C), *At-ptc* (D) and *At-hh* (E,F) RNAi embryos. In control embryos (A), the cumulus arrives at the rim of the germ disc by 6 hours (light-blue dots), corresponding to late stage 5. Prevention and delay of cumulus shifts are seen in B-E (the light-blue arrows point to the light-blue dots.) Continued cumulus shifts are seen in C and F. The embryos in C and B are derived from egg sacs produced by female #2 on days 12 and 23, respectively (see Fig. 8H). Scale bar: 200 μm.

smo function in the same pathway. Specific reduction of the target transcripts was also confirmed. The resultant embryos are referred to as *At-hh* and *At-smo* RNAi embryos.

Time-lapse recording of *At-smo* RNAi embryos revealed that in the most severely affected egg sacs, more than 60% of embryos showed defects associated with CM cell migration. The defects were categorized into three types (Fig. 2B,C; see Movie 1 in the supplementary material): the first and the second defects were a prevention and a delay, respectively, of the cumulus shift observed around the center of the germ disc, whereas the third defect was a cumulus shift that continued around the periphery of the germ disc. These three types of defect were also found in *At-hh* RNAi embryos (Fig. 2E,F; see Movie 1 in the supplementary material). However, more than 70% of the embryos showed a normal, or an almost normal, cumulus shift, even in severely affected egg sacs. Owing to the low penetrance of the cumulus-shift phenotypes, we initially failed to identify *At-hh* as positive in the screen described above (see Table S3 in the supplementary material).

In our analyses of serial egg sacs from females injected with *At-smo* dsRNA (Fig. 2B,C; see also Fig. 8H), we noticed that prevention of cumulus shift was observed only around the time that the maximum effect of RNAi was expected (around the twentieth day from the start of injection, when four injections were performed) (Akiyama-Oda and Oda, 2006; Oda et al., 2007). By contrast, the delayed and continued cumulus-shift defects were observed in a wider time window, and the proportion of the latter decreased around the twentieth day. Based on these observations, we concluded that the prevention of cumulus shift reflects a severe effect of *At-smo* RNAi, whereas the continued shift reflects a mild effect, and the delayed shift an intermediate effect.

The CM cells in *At-ptc*, *At-hh* and *At-smo* RNAi embryos have normal morphology and undergo normal differentiation

We next examined whether the CM cells formed normally in *At-ptc*, *At-hh* and *At-smo* RNAi embryos. As revealed by phalloidin staining, the CM cells showed normal internalization and clustering and a normal distribution of F-actin (Fig. 3A). No abnormalities were observed in the configuration of the surface epithelium around the closed blastopore (data not shown). Staining for the CM cell markers 022_P10 and *At-dpp* and for phosphorylated (p) Mad showed that the CM cells differentiated normally in these RNAi embryos and that they acted as the source of the Dpp signal (Fig. 3B-D).

At-ptc RNAi embryos develop a D-V axis that is parallel to the Em-Ab axis

We examined the consequences of the arrest of the Dpp signal source at the germ disc center in *At-ptc* RNAi embryos. The D-V pattern elements are arranged in the order: the extraembryonic tissue, the *At-gataC* expression domain and the *At-short gastrulation* (*At-sog*) expression domain (Fig. 4A,B). Observation of these D-V pattern elements in *At-ptc* RNAi embryos showed that although a D-V axis developed, it was oriented in parallel to the Em-Ab axis (Fig. 4C,D). Normally, expression of *At-sog*, which encodes a Dpp antagonist, is confined to the ventral midline region of the elongating germ band, where *At-single-minded* (*At-sim*) is subsequently expressed (Akiyama-Oda and Oda, 2006). In the *At-ptc* RNAi embryo, this process appeared to take place in the apical region where expression of the anterior marker *At-orthodenticle* (*At-otd*) was observed (Fig. 4E-G). These results indicated that the *At-ptc* RNAi embryo failed to orthogonalize the major embryonic axes. This was consistent with the expression pattern of the segment marker *At-engrailed* (*At-en*), which was expressed in concentric circles (Fig. 4H). Taken together, these data suggested that the cumulus shift is a crucial step in the formation of the bilaterally symmetric body pattern.

At-hh and *At-smo* RNAi embryos fail to develop a D-V axis

In *At-hh* and *At-smo* RNAi embryos, regardless of CM cell migration, the germ disc gradually shrank during and after stage 6 and failed to form a germ band (see Movie 1 in the supplementary material). Although the relative quantity of *At-dpp* transcripts was not much changed in these RNAi embryos (see Fig. S3D in the supplementary material), the D-V pattern did not develop (Fig. 4I). *At-sog* expression decreased, and the *At-gataC* expression domain failed to form. This condition was in contrast to the clear D-V

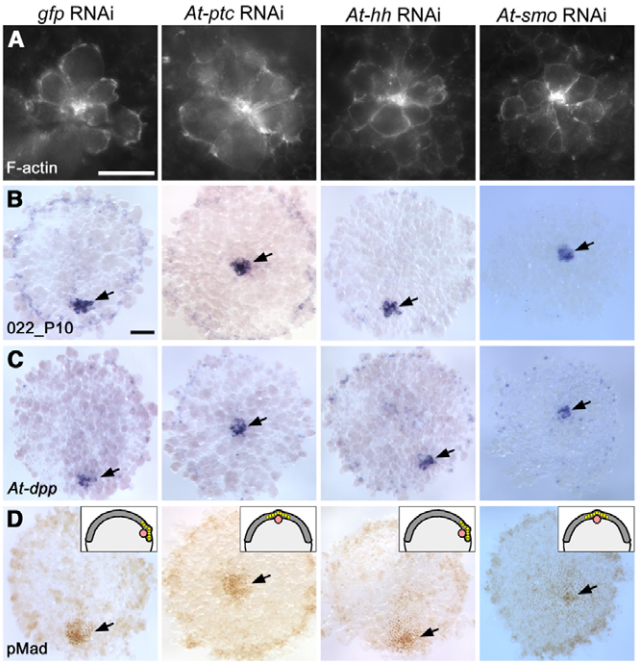

Fig. 3. Normal differentiation of CM cells in *At-ptc*, *At-hh* and *At-smo* RNAi embryos. (**A**) F-actin staining of CM cells in *gfp*, *At-ptc*, *At-hh* and *At-smo* RNAi embryos at early stage 5. (**B-D**) Late stage 5 *gfp*, *At-ptc*, *At-hh* and *At-smo* RNAi embryos stained for 022_P10 (B), *At-dpp* (C) and pMad (D). All germ discs were flat-mounted. Illustrations in D depict the position of CM cells (orange) and pMad-positive nuclei (yellow). Arrows indicate the position of CM cells. Scale bars: 50 μm in A; 100 μm in B-D.

pattern that developed in *At-ptc* RNAi embryos (Fig. 4C,D). These data suggested that *At-hh* and *At-smo*, but not *At-ptc*, are necessary for the progression of D-V axis development.

At-ptc, *At-hh* and *At-smo* RNAi embryos are defective in A-P axis formation

To further investigate the contribution of Hh signaling to axis formation, we examined late stage 7 embryos. At this stage, there is normally expression of the anterior (*At-otd*) and caudal [*At-caudal* (*At-cad*)] markers on the opposite sides of the extending germ bands (Fig. 5A). *At-ptc* RNAi embryos lacked *At-cad* but not *At-otd* expression. Conversely, *At-hh* and *At-smo* RNAi embryos lacked *At-otd* but not *At-cad* expression. Furthermore, the majority of *At-hh* and *At-smo* RNAi embryos had a greatly expanded *At-cad* expression domain. These data suggested that *At-ptc* is required for posterior patterning and that *At-hh* and *At-smo* are required for anterior patterning. The data also suggested that *At-hh* and *At-smo* are involved in the repression of caudal fate.

Notably, *At-ptc* RNAi embryos showed only two *At-en* stripes at late stage 8; this contrasts with wild-type embryos at the same stage, which had more than seven stripes (Fig. 4H), and with *At-hh* and *At-smo* RNAi embryos, which showed no *At-en* expression (Fig. 5B). These results suggested that Hh signaling is involved in segmentation of the spider embryo.

At-ptc, *At-hh* and *At-smo* are expressed in early embryos

To better understand the phenotypic data, we examined the expression of *At-ptc*, *At-hh* and *At-smo* transcripts during early stages of embryonic development. WISH could not be used in stage

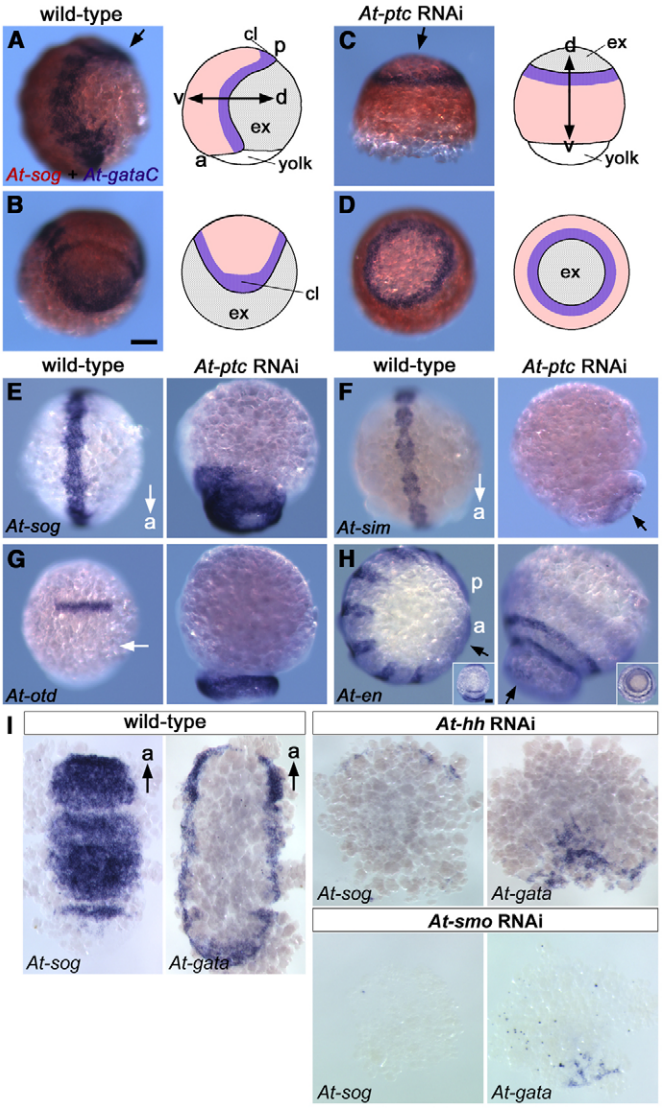

Fig. 4. Effects of *At-ptc*, *At-hh* and *At-smo* RNAi on D-V axis development. (**A-D**) Detection of *At-sog* (red) and *At-gataC* (purple) transcripts in wild-type (A,B) and *At-ptc* RNAi (C,D) embryos at late stage 7. The arrows in A and C indicate the angle at which the embryos were photographed in B and D. (**E-H**) Detection of *At-sog* (E), *At-sim* (F), *At-otd* (G) and *At-en* (H) transcripts in wild-type and *At-ptc* RNAi embryos at late stage 8 (E,G,H) and stage 9 (F). Embryos are viewed from the ventral (wild type in E-G) or lateral (other panels) sides. The black arrow in F indicates the apical region where *At-sim* expression was detected. The white arrow in G indicates the anterior limit of the germ band. Insets in H show the same embryos viewed from the directions indicated by the arrows. (**I**) Detection of *At-sog* and *At-gataC* transcripts in flat-mounted wild-type, *At-hh* RNAi and *At-smo* RNAi embryos at late stage 7. a, anterior; p, posterior; d, dorsal; v, ventral; cl, caudal lobe; ex, extraembryonic tissue. Scale bars: 100 μm.

1 and 2 embryos owing to technical problems with the fixation process. Using RT-PCR, *At-ptc* and *At-smo* transcripts were detected at considerable levels in stage 1 embryos, but *At-hh* transcripts were not detected (see Fig. S4 in the supplementary material). Stage 2 was the earliest stage at which *At-hh* transcripts could be detected by RT-PCR. These data suggested that *At-ptc* and *At-smo* transcripts, but not *At-hh* transcripts, might be maternally loaded in the egg.

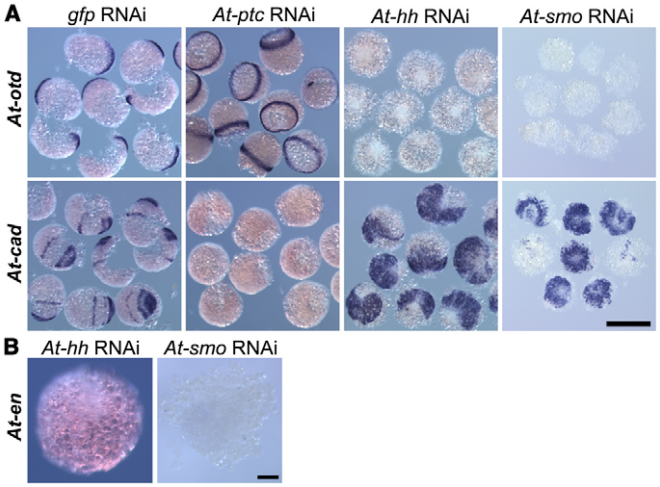

Fig. 5. Effects of *At-ptc*, *At-hh* and *At-smo* RNAi on A-P patterning in the germ band. (**A**) Detection of *At-otd* and *At-cad* transcripts in *gfp*, *At-ptc*, *At-hh* and *At-smo* RNAi embryos at late stage 7. Embryos for each RNAi treatment were derived from the same egg sac. (**B**) Detection of *At-en* transcripts in *At-hh* and *At-smo* RNAi embryos at late stage 8. Compare these with Fig. 4H. Scale bars: 500 μm in A; 100 μm in B.

At-hh expression was observed on the Ab side of the embryo at stage 3 (Fig. 6A), and expression was restricted to the rim of the germ disc by early stage 5 (Fig. 6B). *At-ptc* transcripts were detected in cells located on the Em side at stage 3, with the highest levels in cells near the blastopore region (Fig. 6E). In the blastopore region, we observed cells that expressed both *At-ptc* and the CM-cell marker (Fig. 6N,N′), although it was unclear whether these cells were future CM cells. Ubiquitous expression of *At-ptc* transcripts was observed in the germ disc epithelium at stage 4 (Fig. 6F). However, this expression pattern gradually changed during stage 5, when expression was reduced in the central region of the germ disc and was enhanced in the peripheral region adjacent to the *At-hh*-expressing circular domain (Fig. 6I,O-Q). The reduction of *At-ptc* expression preceded the expansion of the *At-Delta* expression domain from the center (Fig. 6S,T). The expression patterns of *At-hh* and *At-ptc* in the germ disc did not show any asymmetry with respect to the position of the migrating CM cells during stage 5 (Fig. 6L,M,O-R), although a few *At-ptc*-positive cells were irregularly scattered near the germ disc center in about half of the stage 5 embryos examined (Fig. 6I).

During stage 6, the forming caudal lobe initiated *At-hh* and *At-ptc* expression, whereas the anterior region of the forming germ band, which is related to the germ disc peripheral region, showed a stripe of *At-hh* expression flanked with stripes of *At-ptc* expression (Fig. 6C,G,J). The position of the *At-hh* stripe relative to the anterior rim was shifted several cell widths to the posterior after stage 5 (Fig. 6B,C). Later, the formed germ band exhibited segmental stripes of expression of these genes (Fig. 6D,H,K), as is seen in *Drosophila* (Hooper and Scott, 1989; Lee et al., 1992; Nakano et al., 1989; Tabata et al., 1992). Although *At-smo* transcripts were detected during the early stages by RT-PCR (see Fig. S4 in the supplementary material), a specific *At-smo* expression pattern was not detected by WISH.

The expression pattern of *At-hh* was examined in *At-Delta* and *At-smo* RNAi embryos. Like *At-hh*, *At-Delta* is initially expressed on the Ab side of the embryo (Oda et al., 2007). The initial *At-hh*

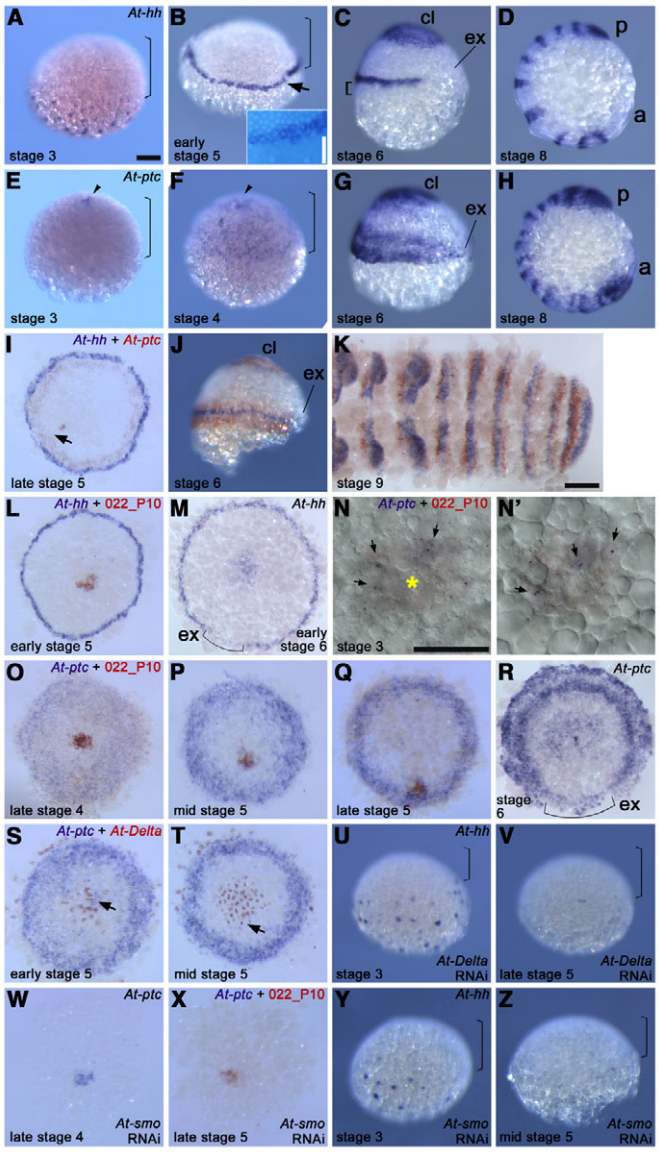

Fig. 6. Expression patterns of *At-hh* and *At-ptc* transcripts revealed by WISH. (**A-T**) Detection of *At-hh* (A-D,M), *At-ptc* (E-H,R), *At-hh* (purple) and *At-ptc* (red) (I-K), *At-hh* (purple) and the CM cell marker 022_P10 (red) (L), *At-ptc* (purple) and 022_P10 (red) (N-Q), and *At-ptc* (purple) and *At-Delta* (red) (S,T) transcripts in wild-type embryos at the indicated stages. A-H and J are lateral views; I and L-T are top views of flat-mounted germ discs; K shows the posterior half of a germ band. The peripheral region of the germ disc (B, arrow) is magnified in the inset, which shows DNA staining. N and N′ show the blastopore region; the focal planes are at the superficial (N) and two-cell deeper (N′) levels. Arrows in N and N′ indicate double-positive cells, and the yellow asterisk in N indicates the blastopore. Brackets indicate the forming or formed germ disc (A,B,E,F), a space between the line of *At-hh* expression and the anterior rim of the forming germ band (C), and differentiating extraembryonic tissue (M,R). Arrowheads indicate the blastopore (E,F), and arrows indicate the position of CM cells (I,S,T). (**U-Z**) Lateral views of *At-Delta* (U,V) and *At-smo* (Y,Z) RNAi embryos stained for *At-hh*, and top views of flat-mounted *At-smo* RNAi germ discs stained for *At-ptc* (W) and double stained for *At-ptc* (purple) and 022_P10 (red) (X) at the indicated stages. Brackets indicate the forming or formed germ disc (U,V,Y,Z). cl, caudal lobe; ex, extraembryonic tissue; a, anterior; p, posterior. Scale bars: 100 μm, except 50 μm in B, inset.

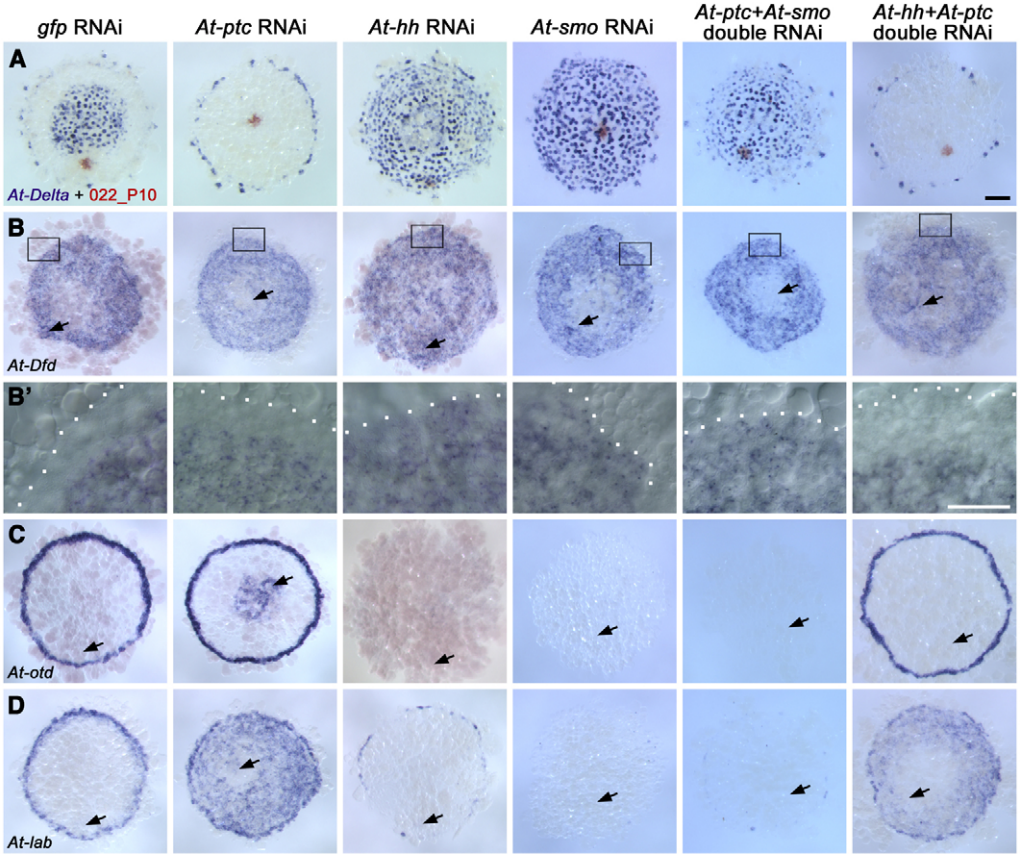

Fig. 7. Effects of *At-ptc*, *At-hh* and *At-smo* RNAi on germ disc patterning. (**A-D**) Detection of *At-Delta* (A, purple) and 022_P10 (A, red), *At-Dfd* (B), *At-otd* (C) and *At-lab* (D) in *gfp*, *At-ptc*, *At-hh* and *At-smo* single-RNAi embryos and in *At-ptc* + *At-smo* and *At-hh* + *At-ptc* double-RNAi embryos. Flat preparations of germ discs at late stage 5. The boxed areas in B are magnified in B′; white dots indicate the border of the germ disc and yolk regions. Arrows indicate the position of CM cells. Scale bars: 100 μm, except 50 μm in B′.

expression on the Ab side of the stage 3 embryo (Fig. 6A) was independent of *At-Delta* and *At-smo* (Fig. 6U,Y), but the later *At-hh* expression at the rim of the germ disc (Fig. 6B,I,L) was dependent on *At-Delta* and *At-smo* (Fig. 6V,Z; see Fig. S3 in the supplementary material). *At-ptc* expression was also examined in *At-smo* RNAi embryos. The *At-ptc* expression at the blastopore region (Fig. 6E,F) was independent of *At-smo* (Fig. 6W), whereas the *At-ptc* expression in the germ disc epithelium (Fig. 6O-Q) was dependent on *At-smo* (Fig. 6W,X). This result is consistent with *ptc* being a known target of Hh signaling (Alexandre et al., 1996; Goodrich et al., 1996; Hidalgo and Ingham, 1990).

Central-peripheral patterning in the germ disc epithelium depends on Hh signaling

The data described above suggested that Hh signaling is involved in the formation of the A-P axis, which is first evident in the germ band (Fig. 5). To investigate the possibility that Hh signaling regulates patterning events in the germ disc, we examined the expression of four distinct regional markers in *At-ptc*, *At-hh* and *At-smo* RNAi germ discs at late stage 5: *At-Delta*, *At-Deformed* (*At-Dfd*), *At-otd* and *At-lab*. *At-Delta* expression, which is normally present in the central region of the germ disc, was expanded to the rim in the *At-hh* and *At-smo* RNAi germ discs; conversely, it was missing entirely in the *At-ptc* RNAi germ disc (Fig. 7A). Early stage 5 *At-ptc* RNAi embryos also lacked the *At-Delta* expression (not shown). These results indicate that *At-ptc*, or negative regulation of Hh signaling, is required for the initiation of *At-Delta* expression around the germ disc center, whereas activation of Hh signaling represses the central fate specification in the peripheral region. Similarly, *At-Dfd* expression, which is normally present in the broad region of the germ disc, except within several cell widths of the periphery, was expanded to the rim in the *At-hh* and *At-smo* RNAi germ discs, although it was normal in the *At-ptc* RNAi germ disc (Fig. 7B,B′). *At-otd* and *At-lab* expression normally appear at and near the rim. The domain of the latter was broader than that of the former, and both overlapped the *At-hh* expression domain (for details, see Fig. S5 in the supplementary material). The *At-otd* expression was missing entirely in the *At-hh* and *At-smo* RNAi germ discs, but was ectopically induced around the central region, with unaffected rim expression, in the *At-ptc* RNAi germ disc (Fig. 7C). The *At-lab* expression was greatly reduced in the *At-hh* and *At-smo* RNAi germ discs and, conversely, was expanded towards the central region in the *At-ptc* RNAi germ disc (Fig. 7D). These results indicated that activation of Hh signaling promotes the specification of peripheral fate. Thus, Hh signaling specifies the central-peripheral pattern in the germ disc, which is related to the caudal-anterior pattern of the germ band. Similarly, the specification of the central and peripheral mesoderm was dependent on Hh signaling, although the specification of central and peripheral endoderm was not (see Fig. S6 in the supplementary material).

Double RNAi for *At-ptc* and *At-smo* yielded phenotypes similar to those of single RNAi for *At-smo*, whereas double RNAi for *At-ptc* and *At-hh* yielded phenotypes similar to those of single RNAi for *At-ptc* (Fig. 7). These epistatic relationships between *At-hh*, *At-ptc* and *At-smo* (*At-hh* → *At-ptc* → *At-smo*) are consistent with established findings in *Drosophila* and vertebrates (Hooper and Scott, 2005; Ingham and McMahon, 2001; Lum and Beachy, 2004).

In RNAi-mediated knockdown experiments, leaky expression of target gene products might be unavoidable. In the case of *At-ptc* single RNAi, there might be residual At-Ptc that is inhibited by At-Hh. In double RNAi for *At-ptc* and *At-hh*, such residual At-Ptc might

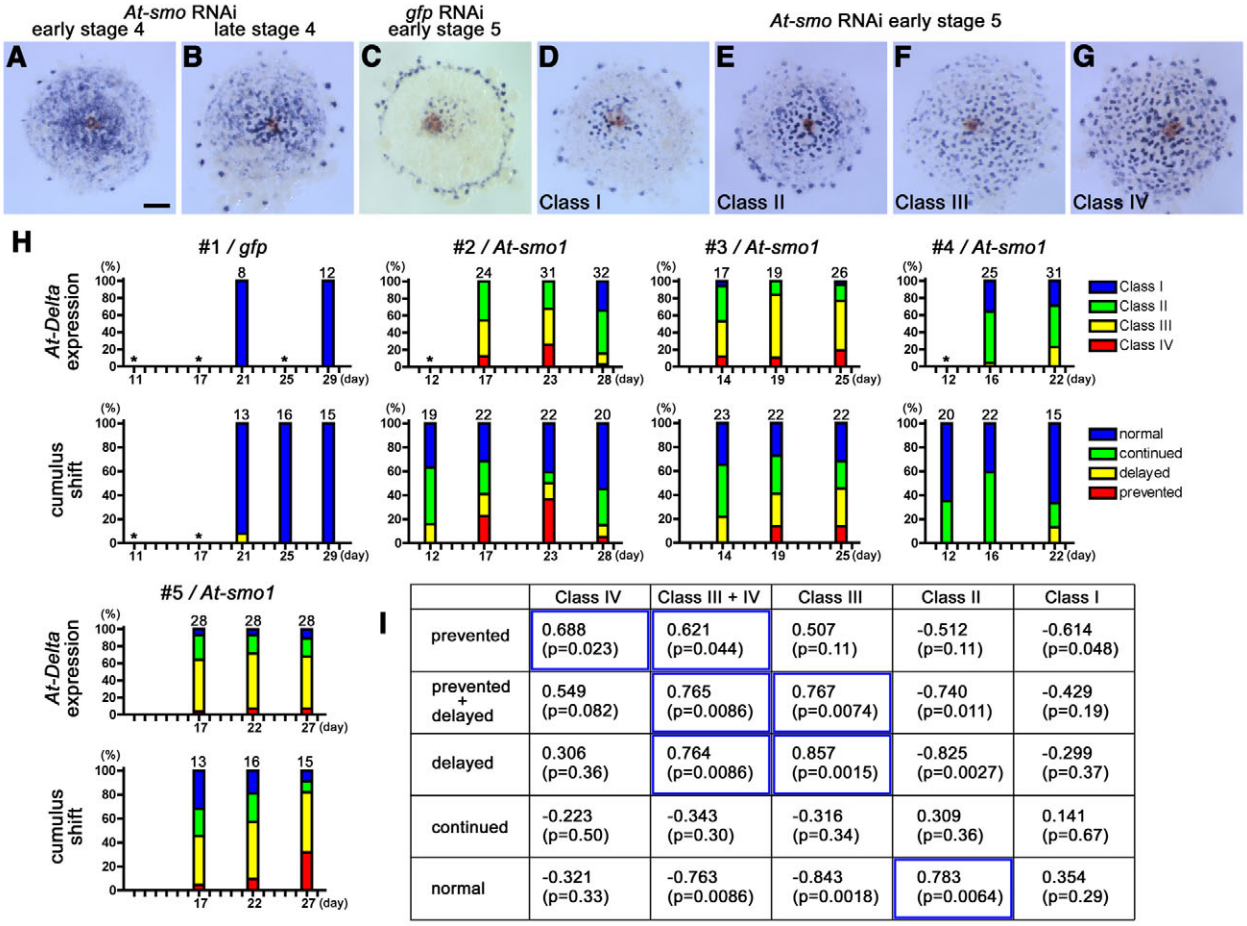

	Class IV	Class III + IV	Class III	Class II	Class I
prevented	0.688 (p=0.023)	0.621 (p=0.044)	0.507 (p=0.11)	-0.512 (p=0.11)	-0.614 (p=0.048)
prevented + delayed	0.549 (p=0.082)	0.765 (p=0.0086)	0.767 (p=0.0074)	-0.740 (p=0.011)	-0.429 (p=0.19)
delayed	0.306 (p=0.36)	0.764 (p=0.0086)	0.857 (p=0.0015)	-0.825 (p=0.0027)	-0.299 (p=0.37)
continued	-0.223 (p=0.50)	-0.343 (p=0.30)	-0.316 (p=0.34)	0.309 (p=0.36)	0.141 (p=0.67)
normal	-0.321 (p=0.33)	-0.763 (p=0.0086)	-0.843 (p=0.0018)	0.783 (p=0.0064)	0.354 (p=0.29)

Fig. 8. Early patterning defects in *At-smo* RNAi germ discs and their relation to the cumulus-shift defects. (**A-G**) Expression of *At-Delta* transcripts (purple) and 022_P10 (red) in *At-smo* RNAi germ discs at early stage 4 (A), late stage 4 (B) and early stage 5 (D-G) and in a *gfp* RNAi germ disc at early stage 5 (C). The germ discs in A and B are derived from the same egg sac produced by female #3 on day 25 (see H). Compare these with the wild-type germ discs in Fig. 1C. The degree of expansion of the *At-Delta* expression domain at early stage 5 was categorized as class I to IV (D-G; see text). Scale bar: 100 μm. (**H**) The percentage of embryos in each *At-Delta* expression phenotype category (above) and with each cumulus-shift phenotype (below) in serial egg sacs. The data in each pair of bar charts refer to individual females (#1-5) injected with *gfp* or *At-smo1* dsRNA. Female #5 was given six injections, whereas the others were given four injections. Bars show data obtained from individual egg sacs produced on the day indicated on the horizontal axis (days after the first injection of dsRNA). At the top of each bar, the total number of examined embryos is indicated. Asterisks indicate egg sacs not examined. (**I**) Spearman correlation matrix of the percentage of embryos in the *At-Delta* expression phenotype categories and the percentage of embryos with the cumulus-shift phenotypes. The correlation was analyzed with Prism version 4 (GraphPad). The Spearman rank correlation coefficients (r_s) are shown together with *P*-values (p). Blue boxes highlight the significant positive correlations.

contribute to the inhibition of At-Smo. With this in mind, one might expect that phenotypes for *At-hh* and *At-ptc* double RNAi are milder than those for *At-ptc* single RNAi and are more like those observed for *At-hh* single RNAi. This is consistent with the absence of central *At-otd* expression and the slight reduction in peripheral *At-otd* expression observed in the double-RNAi germ discs (Fig. 7C). Similar logic may be applied to the *At-ptc* and *At-smo* double RNAi. Thus, the central-peripheral pattern in the germ disc may depend on the activities (and the balance of activities) of the Hh signaling components.

Early predominance of central gene expression in severely affected *At-smo* RNAi germ discs and its correlation with cumulus-shift defects

To understand the process by which a reduction in Hh signaling activity results in greatly expanded *At-Delta* expression in late stage 5 germ discs (Fig. 7A), we examined *At-smo* RNAi embryos at earlier stages. In severe cases, *At-Delta* expression predominated in the germ disc from early stage 4 (Fig. 8A,B). This situation contrasts sharply with that of a normal germ disc, in which little *At-Delta* expression can be observed at early stage 4 (Fig. 1C). These observations suggested that Hh signaling activity is required in the entire germ disc prior to stage 5 for repression of central gene expression.

At early stage 5, when the CM cells begin migration in the normal embryo, *At-smo* RNAi germ discs showed various degrees of expansion of the *At-Delta* expression domain (Fig. 8D-G). To investigate the relationship between the expansion phenotype and the cumulus-shift phenotype (Fig. 2B,C), we analyzed serial egg sacs derived from individual females injected with *At-smo1* dsRNA or *gfp* dsRNA (Fig. 8H). Embryos from each egg sac were divided into two pools. One pool was examined for *At-Delta* expression at early stage 5 and the expansion levels categorized into four classes: class I, comparable to normal; class II, slightly expanded; class III,

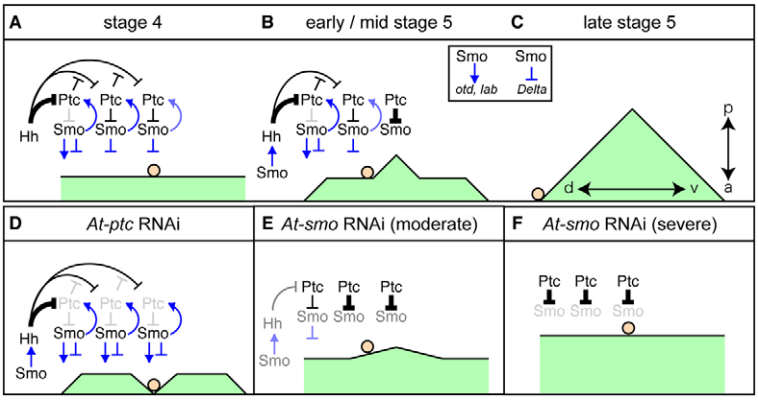

Fig. 9. A model to explain the relationship between germ disc pattern formation and CM cell migration. (**A-C**) Schematics illustrating the process by which Hh signaling forms the central-peripheral pattern in the germ disc (A, stage 4; B, early/mid-stage 5; C, late stage 5). In the green area, the horizontal axis indicates the position along the diameter of the germ disc and the height indicates the hypothetical positional value. The CM cells (orange circle) move down along the emerging positional value gradient. Smo-mediated transcriptional regulation is represented by blue lines, and protein-level regulation between the signaling components is shown by black lines. (**D-F**) The different shapes of the defective positional value gradients that form in *At-ptc* RNAi (D), moderately affected *At-smo* RNAi (E) and severely affected *At-smo* RNAi (F) germ discs at early/mid-stage 5. a, anterior; p, posterior; d, dorsal; v, ventral.

largely, but not fully, expanded (some part of the expression domain reaching the rim); class IV, fully expanded (Fig. 8D-G). The second pool of embryos was examined for the cumulus shift. These analyses revealed that the prevention and delay of cumulus shifts correlated significantly with the expression of the class III and class IV phenotypes (Fig. 8I). These results suggested that the predominant central (or caudal) fate, which is evident at the molecular level prior to stage 5, correlates with a failure to initiate CM cell migration.

DISCUSSION

The early spider embryo as a model for studying cell migration

In this study, we took advantage of the availability of parental RNAi in the spider *Achaearanea tepidariorum* to carry out a function-based screen for genes involved in cell migration during embryogenesis. The knockdown of some genes affected CM cell migration but had no apparent effects on earlier events, such as blastoderm, germ disc and CM cell formation, a finding that validates the use of this unique model system for studying cell migration. A large-scale screen will most likely identify more genes involved in the regulation of CM cell migration. As with border cell migration in the *Drosophila* egg chamber (Montell, 2003; Rørth, 2002), the simplicity of this model system is advantageous, allowing the study of molecular mechanisms that regulate the initiation, direction and termination of cell migration.

CM cell migration is coordinated with pattern formation mediated by Hh signaling

Our data clearly show that Hh signaling is involved in specifying the peripheral-central pattern of the germ disc, similar to the role of Hh signaling in determining the D-V pattern of the vertebrate neural tube (Dessaud et al., 2008). The cell migration defects of *At-ptc* and *At-smo* RNAi embryos correlated with patterning defects in the germ disc. In the central region of the *At-ptc* RNAi germ disc, prevention of CM cell migration was accompanied by a lack of central gene expression and by ectopic expression of peripheral genes. In the peripheral region of the moderately affected *At-smo* RNAi germ disc, continued CM cell migration was accompanied by a lack of peripheral gene expression and by an expansion of central gene expression. Moreover, severely affected *At-smo* RNAi embryos exhibited prevention or delay of CM cell migration. This defect was concurrent with an early predominance of central gene expression over the germ disc. The simultaneous observation of cell migration defects and patterning defects might indicate that CM cell movement is tied to some aspect of positional information. We propose a model that explains the defects caused by perturbations in Hh signaling (Fig. 9).

Hh signaling mediates long-range patterning in a variety of vertebrate and invertebrate tissues (Briscoe et al., 2001; Dessaud et al., 2008; Ingham and McMahon, 2001; Ingham and Placzek, 2006). The predominance of central gene expression in the severely affected *At-smo* RNAi germ disc prior to stage 5 suggests that At-Hh initially travels from its source (the outside and rim of the forming and formed germ disc) up to the central region to repress central gene expression in the normal germ disc (Fig. 9A). Considering that *At-ptc* is a putative target of Hh signaling, this idea is also supported by the observation that *At-ptc* transcripts were ubiquitously distributed in the forming and formed germ discs at stages 3 and 4. The travelling distance of sonic hedgehog (Shh), a vertebrate homolog of Hh, was estimated to be ~300 μm (~30 cell diameters) in the mouse limb bud (Lewis et al., 2001). This distance is comparable to the radius of the *Achaearanea* germ disc. Initial rapid diffusion of the Hh ligand over a long distance has been supported by a simulation study of Shh signaling dynamics in the vertebrate neural tube (Saha and Schaffer, 2006). Our data obtained with *At-Delta* and *At-smo* RNAi embryos implies that the maintenance of the Hh signal source is regulated by Notch signaling and by Hh signaling itself.

Through At-Smo-mediated signal transduction, high levels of At-Hh (short-range signal) promote peripheral gene expression, whereas moderate and low levels of At-Hh (long-range signal) are probably able to repress central gene expression in the germ disc. This repression might be followed by a derepression process that involves *At-ptc* (Fig. 9B). The *ptc* gene is a target of Hh signaling (Alexandre et al., 1996; Goodrich et al., 1996; Hidalgo and Ingham, 1990), and the Ptc protein serves to inhibit Hh transport (Chen and Struhl, 1996; Jeong and McMahon, 2005). These two regulatory mechanisms might account for the progressive derepression of central gene expression from the germ disc center. *At-ptc* transcription is enhanced in more peripheral regions of the germ disc, depending on the distance from the At-Hh signal source. The peripheral At-Ptc inhibits the movement of At-Hh towards the germ disc center, and, accordingly, the central At-Ptc blocks At-Smo activity in progressively more distant regions from the germ disc center, leading to the derepression of central gene expression. This dynamic sequence of signaling events might contribute to determining the shape of the positional value gradient that reflects the future A-P axis (Fig. 9C).

The timing of the derepression of central gene expression is close to that of the initiation of CM cell migration. An important aspect of our model is that the CM cells move down along the emerging positional value gradient. The shape of the positional value gradient might be affected by depletion of components of the Hh signaling network, which may thereby affect the behavior of the CM cells (Fig. 9D-F). In *At-ptc* RNAi embryos, At-Smo is activated throughout the entire germ disc and the derepression mechanism fails to function, as the peak of the gradient is not formed at the germ disc center. The ectopic *At-otd* expression implies that the slope of the gradient may be reversed around the germ disc center and also that the terminal patterning system might function as in *Drosophila* (Finkelstein and Perrimon, 1990). In the *At-smo* RNAi embryos, the slope of the gradient may be reduced depending on the level of residual At-Smo activities. The reversed polarity and reduced slope of the positional value gradient around the germ disc center might result in the delay or prevention of CM cell migration. The defect in the termination of CM cell migration in the *At-smo* RNAi embryo might be attributable to a lack of a 'stop signal' associated with peripheral cell fate or to local positional value gradients potentially formed along the circumference of the germ disc.

More studies are needed to elucidate the molecular basis of the proposed positional value gradient. It is possible that concentrations of extracellular Hh or of other components of the Hh signaling network directly relate to the positional values. Previous studies proposed that Hh and Shh induce and restrict cell migration (Bijlsma et al., 2007; Deshpande et al., 2001; Fu et al., 2004). In particular, it was shown in vitro that mouse mesenchymal fibroblasts migrate towards an Shh gradient in a transcription-independent manner (Bijlsma et al., 2007). However, our data provide no evidence that At-Hh serves as a guiding cue for CM cell migration. Alternatively, secreted or cell-surface proteins expressed under the control of Hh signaling might be involved in the positional information that affects the CM cells. Although expression of *At-Delta* is controlled by Hh signaling, its knockdown does not affect CM cell migration (Oda et al., 2007). To test our hypotheses, technical advances, as well as the identification of more of the genes involved in the cell migration, are needed.

Evolution of developmental mechanisms for axis formation

This study provides the first evidence that Hh signaling mediates the formation of the two major embryonic axes, the A-P and D-V axes, in a bilaterally symmetric animal. However, the importance of Hh signaling has been documented for tissue-level axis formation in *Drosophila* and vertebrates (Ingham and McMahon, 2001; Tabata, 2001). The roles that the *Achaearanea* Hh system plays in germ disc patterning are similar to those played by *Drosophila* Bicoid in A-P patterning (Driever and Nüsslein-Volhard, 1988). The former is based on the diffusion of extracellular signals in a cell-based embryo, and the latter is based on the diffusion of transcription factors in a syncytial embryo. This striking contrast indicates that drastic changes in developmental programs can occur without disrupting the basic arthropod body plan.

There is another important difference between *Drosophila* and *Achaearanea* in the cellular and molecular mechanisms that orthogonalize the two embryonic axes. In *Drosophila*, migration of the nucleus in the oocyte localizes the source of the Gurken signal, a TGFα-like protein (Neuman-Silberberg and Schüpbach, 1993), to an asymmetric position with respect to the primary axis, and this specifies the orientation of the D-V axis (Roth, 2003; van Eeden and St Johnston, 1999). Through many subsequent steps, the domain of *dpp* transcription is determined on the dorsal side of the blastoderm embryo (Morisato and Anderson, 1995). The corresponding symmetry-breaking event in *Achaearanea* appears to be the migration of the CM cells, which express the evolutionarily conserved dorsal signal Dpp, in the germ disc stage embryo (Oda and Akiyama-Oda, 2008). Thus far, no genes have been found that are expressed asymmetrically in the germ disc stage embryo prior to CM cell migration. Our model (Fig. 9) predicts that the initial direction of migration of the CM cells is determined through stochastic processes related to Hh signaling network dynamics. Stochastic processes have also been proposed to determine the direction of migration of the *Drosophila* oocyte nucleus (Roth et al., 1999). Despite the differences in the components, the basic principles of axis formation seem to be similar between even these phylogenetically distant arthropods. As in spiders, cell migration plays a key role in mammalian embryonic axis formation (Beddington and Robertson, 1999; Kimura-Yoshida et al., 2005; Yamamoto et al., 2004). Recent studies in planaria show that Hh signaling functions in establishing A-P polarity in regenerating tissues (Rink et al., 2009; Yazawa et al., 2009). Studies in the simple spider model could contribute to a better understanding of common aspects of axis formation in bilateria and of early evolution of the bilaterian body plan.

Acknowledgements

We thank T. Tabata for antibody, K. Agata and H. Tarui for EST clones, M. Kanayama for *Delta* RNAi samples, A. Noda for technical assistance and K. Agata for critical reading of the manuscript. This work was partly supported by JSPS and MEXT KAKENHI to Y.A. and H.O. Y.A. is a JSPS Research Fellow.

Competing interests statement

The authors declare no competing financial interests.

Supplementary material

Supplementary material for this article is available at
http://dev.biologists.org/lookup/suppl/doi:10.1242/dev.045625/-/DC1

References

Akiyama-Oda, Y. and Oda, H. (2003). Early patterning of the spider embryo: a cluster of mesenchymal cells at the cumulus produces Dpp signals received by germ disc epithelial cells. *Development* **130**, 1735-1747.

Akiyama-Oda, Y. and Oda, H. (2006). Axis specification in the spider embryo: *dpp* is required for radial-to-axial symmetry transformation and *sog* for ventral patterning. *Development* **133**, 2347-2357.

Alcedo, J., Ayzenzon, M., Von Ohlen, T., Noll, M. and Hooper, J. E. (1996). The Drosophila *smoothened* gene encodes a seven-pass membrane protein, a putative receptor for the Hedgehog signal. *Cell* **86**, 221-232.

Alexandre, C., Jacinto, A. and Ingham, P. W. (1996). Transcriptional activation of *hedgehog* target genes in *Drosophila* is mediated directly by the Cubitus interruptus protein, a member of the GLI family of zinc finger DNA-binding proteins. *Genes Dev.* **10**, 2003-2013.

Beddington, R. S. and Robertson, E. J. (1999). Axis development and early asymmetry in mammals. *Cell* **96**, 195-209.

Bijlsma, M. F., Borensztajn, K. S., Roelink, H., Peppelenbosch, M. P. and Spek, C. A. (2007). Sonic hedgehog induces transcription-independent cytoskeletal rearrangement and migration regulated by arachidonate metabolites. *Cell. Signal.* **19**, 2596-2604.

Briscoe, J., Chen, Y., Jessell, T. M. and Struhl, G. (2001). A hedgehog-insensitive form of patched provides evidence for direct long-range morphogen activity of sonic hedgehog in the neural tube. *Mol. Cell* **7**, 1279-1291.

Chen, Y. and Struhl, G. (1996). Dual roles for patched in sequestering and transducing Hedgehog. *Cell* **87**, 553-563.

Cram, E. J., Shang, H. and Schwarzbauer, J. E. (2006). A systematic RNA interference screen reveals a cell migration gene network in *C. elegans*. *J. Cell Sci.* **119**, 4811-4818.

Deshpande, G., Swanhart, L., Chiang, P. and Schedl, P. (2001). Hedgehog signaling in germ cell migration. *Cell* **106**, 759-769.

Dessaud, E., McMahon, A. P. and Briscoe, J. (2008). Pattern formation in the vertebrate neural tube: a sonic hedgehog morphogen-regulated transcriptional network. *Development* **135**, 2489-2503.

Driever, W. and Nüsslein-Volhard, C. (1988). The *bicoid* protein determines position in the Drosophila embryo in a concentration-dependent manner. *Cell* **54**, 95-104.

Finkelstein, R. and Perrimon, N. (1990). The *orthodenticle* gene is regulated by *bicoid* and *torso* and specifies *Drosophila* head development. *Nature* **346**, 485-488.
Fu, M., Lui, V. C., Sham, M. H., Pachnis, V. and Tam, P. K. (2004). Sonic hedgehog regulates the proliferation, differentiation, and migration of enteric neural crest cells in gut. *J. Cell Biol.* **166**, 673-684.
Fuse, N., Maiti, T., Wang, B., Porter, J. A., Hall, T. M., Leahy, D. J. and Beachy, P. A. (1999). Sonic hedgehog protein signals not as a hydrolytic enzyme but as an apparent ligand for patched. *Proc. Natl. Acad. Sci. USA* **96**, 10992-10999.
Goodrich, L. V., Johnson, R. L., Milenkovic, L., McMahon, J. A. and Scott, M. P. (1996). Conservation of the hedgehog/patched signaling pathway from flies to mice: induction of a mouse patched gene by Hedgehog. *Genes Dev.* **10**, 301-312.
Hidalgo, A. and Ingham, P. (1990). Cell patterning in the *Drosophila* segment: spatial regulation of the segment polarity gene *patched*. *Development* **110**, 291-301.
Hooper, J. E. and Scott, M. P. (1989). The Drosophila *patched* gene encodes a putative membrane protein required for segmental patterning. *Cell* **59**, 751-765.
Hooper, J. E. and Scott, M. P. (2005). Communicating with Hedgehogs. *Nat. Rev. Mol. Cell Biol.* **6**, 306-317.
Ingham, P. W. and McMahon, A. P. (2001). Hedgehog signaling in animal development: paradigms and principles. *Genes Dev.* **15**, 3059-3087.
Ingham, P. W. and Placzek, M. (2006). Orchestrating ontogenesis: variations on a theme by sonic hedgehog. *Nat. Rev. Genet.* **7**, 841-850.
Ingham, P. W., Taylor, A. M. and Nakano, Y. (1991). Role of the *Drosophila patched* gene in positional signalling. *Nature* **353**, 184-187.
Jeong, J. and McMahon, A. P. (2005). Growth and pattern of the mammalian neural tube are governed by partially overlapping feedback activities of the hedgehog antagonists patched 1 and Hhip1. *Development* **132**, 143-154.
Kimura-Yoshida, C., Nakano, H., Okamura, D., Nakao, K., Yonemura, S., Belo, J. A., Aizawa, S., Matsui, Y. and Matsuo, I. (2005). Canonical Wnt signaling and its antagonist regulate anterior-posterior axis polarization by guiding cell migration in mouse visceral endoderm. *Dev. Cell* **9**, 639-650.
Lee, J. J., von Kessler, D. P., Parks, S. and Beachy, P. A. (1992). Secretion and localized transcription suggest a role in positional signaling for products of the segmentation gene *hedgehog*. *Cell* **71**, 33-50.
Lewis, P. M., Dunn, M. P., McMahon, J. A., Logan, M., Martin, J. F., St-Jacques, B. and McMahon, A. P. (2001). Cholesterol modification of sonic hedgehog is required for long-range signaling activity and effective modulation of signaling by Ptc1. *Cell* **105**, 599-612.
Lum, L. and Beachy, P. A. (2004). The Hedgehog response network: sensors, switches, and routers. *Science* **304**, 1755-1759.
Marigo, V., Davey, R. A., Zuo, Y., Cunningham, J. M. and Tabin, C. J. (1996). Biochemical evidence that patched is the Hedgehog receptor. *Nature* **384**, 176-179.
Montell, D. J. (2003). Border-cell migration: the race is on. *Nat. Rev. Mol. Cell Biol.* **4**, 13-24.
Morisato, D. and Anderson, K. V. (1995). Signaling pathways that establish the dorsal-ventral pattern of the *Drosophila* embryo. *Annu. Rev. Genet.* **29**, 371-399.
Nakano, Y., Guerrero, I., Hidalgo, A., Taylor, A., Whittle, J. R. and Ingham, P. W. (1989). A protein with several possible membrane-spanning domains encoded by the *Drosophila* segment polarity gene patched. *Nature* **341**, 508-513.
Neuman-Silberberg, F. S. and Schüpbach, T. (1993). The Drosophila dorsoventral patterning gene *gurken* produces a dorsally localized RNA and encodes a TGF α-like protein. *Cell* **75**, 165-174.
Oda, H. and Akiyama-Oda, Y. (2008). Differing strategies for forming the arthropod body plan: lessons from Dpp, Sog and Delta in the fly *Drosophila* and spider *Achaearanea*. *Dev. Growth Differ.* **50**, 203-214.
Oda, H., Nishimura, O., Hirao, Y., Tarui, H., Agata, K. and Akiyama-Oda, Y. (2007). Progressive activation of Delta-Notch signaling from around the blastopore is required to set up a functional caudal lobe in the spider *Achaearanea tepidariorum*. *Development* **134**, 2195-2205.
Persson, U., Izumi, H., Souchelnytskyi, S., Itoh, S., Grimsby, S., Engström, U., Heldin, C. H., Funa, K. and ten Dijke, P. (1998). The L45 loop in type I receptors for TGF-β family members is a critical determinant in specifying Smad isoform activation. *FEBS Lett.* **434**, 83-87.
Rink, J. C., Gurley, K. A., Elliott, S. A. and Sánchez Alvarado, A. (2009). Planarian Hh signaling regulates regeneration polarity and links Hh pathway evolution to cilia. *Science* **326**, 1406-1410.
Rørth, P. (2002). Initiating and guiding migration: lessons from border cells. *Trends Cell Biol.* **12**, 325-331.
Roth, S. (2003). The origin of dorsoventral polarity in *Drosophila*. *Philos. Trans. R. Soc. Lond. B, Biol. Sci.* **358**, 1317-1329.
Roth, S., Jordan, P. and Karess, R. (1999). Binuclear *Drosophila* oocytes: consequences and implications for dorsal-ventral patterning in oogenesis and embryogenesis. *Development* **126**, 927-934.
Saha, K. and Schaffer, D. V. (2006). Signal dynamics in Sonic hedgehog tissue patterning. *Development* **133**, 889-900.
Saitou, N. and Nei, M. (1987). The Neighbor-joining method: a new method for reconstructing phylogenetic trees. *Mol. Biol. Evol.* **4**, 406-425.
Simpson, K. J., Selfors, L. M., Bui, J., Reynolds, A., Leake, D., Khvorova, A. and Brugge, J. S. (2008). Identification of genes that regulate epithelial cell migration using an siRNA screening approach. *Nat. Cell Biol.* **10**, 1027-1038.
Solnica-Krezel, L. (2005). Conserved patterns of cell movements during vertebrate gastrulation. *Curr. Biol.* **15**, R213-R228.
Stone, D. M., Hynes, M., Armanini, M., Swanson, T. A., Gu, Q., Johnson, R. L., Scott, M. P., Pennica, D., Goddard, A. et al. (1996). The tumour-suppressor gene patched encodes a candidate receptor for Sonic hedgehog. *Nature* **384**, 129-134.
Tabata, T. (2001). Genetics of morphogen gradients. *Nat. Rev. Genet.* **2**, 620-630.
Tabata, T., Eaton, S. and Kornberg, T. B. (1992). The *Drosophila hedgehog* gene is expressed specifically in posterior compartment cells and is a target of *engrailed* regulation. *Genes Dev.* **6**, 2635-2645.
Taipale, J., Cooper, M. K., Maiti, T. and Beachy, P. A. (2002). Patched acts catalytically to suppress the activity of Smoothened. *Nature* **418**, 892-897.
Tam, P. P., Loebel, D. A. and Tanaka, S. S. (2006). Building the mouse gastrula: signals, asymmetry and lineages. *Curr. Opin. Genet. Dev.* **16**, 419-425.
van den Heuvel, M. and Ingham, P. W. (1996). *smoothened* encodes a receptor-like serpentine protein required for *hedgehog* signalling. *Nature* **382**, 547-551.
van Eeden, F. and St Johnston, D. (1999). The polarisation of the anterior-posterior and dorsal-ventral axes during *Drosophila* oogenesis. *Curr. Opin. Genet. Dev.* **9**, 396-404.
Wang, X., Bo, J., Bridges, T., Dugan, K. D., Pan, T. C., Chodosh, L. A. and Montell, D. J. (2006). Analysis of cell migration using whole-genome expression profiling of migratory cells in the *Drosophila* ovary. *Dev. Cell* **10**, 483-495.
Yamamoto, M., Saijoh, Y., Perea-Gomez, A., Shawlot, W., Behringer, R. R., Ang, S. L., Hamada, H. and Meno, C. (2004). Nodal antagonists regulate formation of the anteroposterior axis of the mouse embryo. *Nature* **428**, 387-392.
Yamazaki, K., Akiyama-Oda, Y. and Oda, H. (2005). Expression patterns of a *twist*-related gene in embryos of the spider *Achaearanea tepidariorum* reveal divergent aspects of mesoderm development in the fly and spider. *Zool. Sci.* **22**, 177-185.
Yazawa, S., Umesono, Y., Hayashi, T., Tarui, H. and Agata, K. (2009). Planarian Hedgehog/Patched establishes anterior-posterior polarity by regulating Wnt signaling. *Proc. Natl. Acad. Sci. USA* **106**, 22329-22334.

Table S1. cDNAs used in this study

cDNA (symbol)	Protein type or motif	Accession number	Ref.*
At-patched (*ptc*)	Multi-transmembrane Hh receptor	AB433900	1
At-hedgehog (*hh*)	Secreted signaling molecule	AB125742	2
At-smoothened (*smo*)	Seven-transmembrane protein	AB524079	1
At-caudal (*cad*)	Homeodomain	AB096075	3
At-decapentaplegic (*dpp*)	Secreted signaling molecule	AB096072	3
At-Delta	Transmembrane Notch ligand	AB287420	2
At-engrailed (*en*)	Homeodomain	AB125741	4
At-gataC	Zinc finger	AB433902	1
At-labial (*lab*)	Homeodomain (Hox1)	AB433903	1
At-orthodenticle (*otd*)	Homeodomain	AB096074	3
At-short gastrulation (*sog*)	Secreted Dpp antagonist	AB236147	4
At-single-minded (*sim*)	PAS domain	AB236150	4
At-twist (*twi*)	Basic helix-loop-helix	AB167807	5
At-Deformed (*Dfd*) (At_eW_016_B10)	Homeodomain (Hox4)	AB433904	1, 2
CM-cell marker (At_eW_022_P10)	Fascin-like domain (Singed)	AB433905	1, 2
Endoderm marker (At_eW_012_A08)	Glycerophosphoryl diester phosphodiesterase	AB433906	1, 2
At-α-catenin (At_eW_003_D02)	Vinculin family	AB433907	1, 2
At-ef1α (At_eW_003_E07)	Elongation factor 1α	AB433908	1, 2

*References: 1, this study; 2, Oda et al. (2007); 3, Akiyama-Oda and Oda (2003); 4, Akiyama-Oda and Oda (2006); 5, Yamazaki et al. (2005).

Table S2. Primers used in this study

	Nucleotide sequence* (5′ to 3′)	Amino acid sequence
Degenerate primer		
At-ptc forward	AARYTNYTNGTNCARACNGG	KLLVQTG
At-ptc reverse	TGYTCCCARAANARRAANGG	PFLFWEQ
At-smo forward	TGYTGGGCNGYNATHCARCC	CWA(A/V)IQP
At-smo reverse	TANCCNACRAARCADATNCC	GICFVGY
At-lab forward†	GNACNAAYTTYACNAAYAARCA	RTNFTNKQ
At-lab forward-2†	GARYTNGARAARGARTTYCA	ELEKEFH
At-lab reverse†	CATNCKNCKRTTYTGRAACCA	WFQNRRM
At-gataC forward	GNGARTGYGTNAAYTGYGG	RECVNCG
At-gataC reverse	GCRTTRCANACNGGYTCNCC	GEPVCNA
RACE primer		
At-ptc 5′RACE-1‡	CGTGTGTCCAGCGACGAGGTTCTGGCA	
At-ptc 5′RACE-2‡	TCTGGTCCGAGAAGCTTTGAGCCTTCC	
At-ptc 3′RACE	TGCCAGAACCTCGTCGCTGGACACACG	
At-smo 5′RACE	GGATTCTGGCATGGCACTCCACAACC	
At-smo 3′RACE-1‡	GGTTGTGGAGTGCCATGCCAGAATCC	
At-smo 3′RACE-2‡	GACGCATGTCCCTCCCGGAATCATC	
At-lab 5′RACE	CGTTTCATTGAGGCCAAGAGAAGAGGC	
At-lab 3′RACE	GCCTCTTCTCTTGGCCTCAATGAAACG	
At-gataC 5′RACE	TCGCCGCGGACAGTCGCCTCTTGG	
At-gataC 3′RACE	GGAGAGCGGGTACGAGCTGCGCGA	

*D is A, G or T; H is A, C or T; K is G or T; M is A or C; N is A, C, G or T; R is A or G; Y is C or T.

†For cloning of *At-lab*, *At-lab* forward and *At-lab* reverse primers were used for the first PCR, and *At-lab* forward-2 and *At-lab* reverse were used for the second PCR.

‡PCR using the first primer resulted in partial clones. The second primer was used to obtain the full sequence.

Table S3. Gene fragments tested in the pilot screen

Characteristic of DNA sequence	Eggs obtained?	Germ disc formed?	CM cell migration
hedgehog	Yes	Yes	Normal*
patched	Yes	Yes	Defective
Wnt5	Yes	Yes	Normal
Wnt7	No	–	–
Wnt8	Yes	Yes	Normal
frizzled	Yes	Ambiguous	–
Sizzled	Yes	Ambiguous	–
LDLRR6	No	–	–
BAMBI	Yes	Yes	Normal
ADMP	Yes	Yes	Normal
Activin A receptor, type IIA/B	Yes	Yes	Normal
Keren/Spitz	Yes	Yes	Normal
FGF receptor	Yes	Yes	Normal
Tolloid	Yes	Yes	Normal
crossveinless	Yes	Yes	Normal
mothers against Dpp	No	–	–
SMAD2	No	–	–
SMAD6/7	Yes	Yes	Normal
hairy	Yes	Yes	Normal
Sox-Neuro/Sox2	Yes	Yes	Normal
forkhead	Yes	Yes	Normal
armadillo	No	–	–
Axin	Yes	Ambiguous	–
disheveled	Yes	Yes	Normal
orthodenticle	Yes	Yes	Normal
caudal	Yes	Yes	Normal
Pax3/7	No	–	–
odd-paired/Zic	Yes	Yes	Normal
fushitarazu	Yes	Yes	Normal
scalloped	No	–	–
tailless	Yes	Yes	Normal
gataB	No	–	–
gataC	Yes	Yes	Normal

*Close observation revealed defects in migration at low frequencies.